JACS
JOURNAL OF THE AMERICAN CHEMICAL SOCIETY

Article

pubs.acs.org/JACS

Synthesis of Nonequilibrium Supramolecular Peptide Polymers on a Microfluidic Platform

Thomas O. Mason,[†] Thomas C. T. Michaels,[†] Aviad Levin,[‡] Ehud Gazit,[‡,⊥] Christopher M. Dobson,[†] Alexander K. Buell,[*,†,§] and Tuomas P. J. Knowles[*,†]

[†]Department of Chemistry, University of Cambridge, Cambridge CB2 1EW, United Kingdom
[‡]Department for Molecular Microbiology and Biotechnology, University of Tel Aviv, Tel Aviv 6997801, Israel
[§]Institute of Physical Biology, Heinrich-Heine-University Düsseldorf, Düsseldorf 40225, Germany
[⊥]Department of Materials Science and Engineering, Tel Aviv University, Tel Aviv 6997801, Israel

ABSTRACT: The self-assembly of peptides and peptide mimetics into supramolecular polymers has been established in recent years as a route to biocompatible nanomaterials with novel mechanical, optical, and electronic properties. The morphologies of the resulting polymers are usually dictated by the strengths as well as lifetimes of the noncovalent bonds that lead to the formation of the structures. Together with an often incomplete understanding of the assembly mechanisms, these factors limit the control over the formation of polymers with tailored structures. Here, we have developed a microfluidic flow reactor to measure growth rates directly and accurately on the axial and radial faces of crystalline peptide supramolecular polymers. We show that the structures grow through two-dimensional nucleation mechanisms, with rates that depend exponentially on the concentration of soluble peptide. Using these mechanistic insights into the growth behavior of the axial and radial faces, we have been able to tune the aspect ratio of populations of dipeptide assemblies. These results demonstrate a general strategy to control kinetically self-assembly beyond thermodynamic products governed by the intrinsic properties of the building blocks in order to attain the required morphology and function.

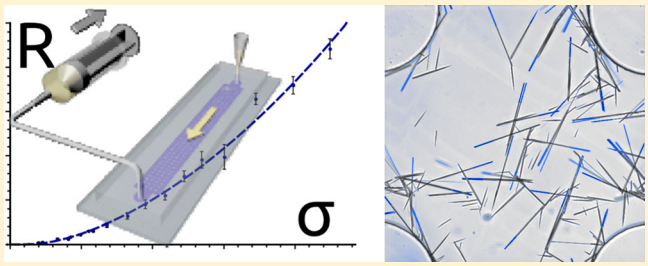

INTRODUCTION

Supramolecular polymers, i.e., polymeric materials that are formed through noncovalent interactions between the building blocks, have been shown to possess a range of advantages over conventional polymers, such as easy processability and self-healing.[1] If the building blocks are based on peptides, the resulting supramolecular polymers can possess biological functionality[2] and be biodegradable. Short peptides can assemble into filamentous, as well as crystalline supramolecular polymers; in some cases a given sequence can assemble into both types of structures, depending on the solution conditions.[3] In particular aromatic dipeptides have been found to be capable of self-assembling in aqueous solution to form highly anisotropic nano- and microcrystalline structures that are reversibly held together by noncovalent interactions. The dynamic nature of the noncovalent interactions allows the formation of organized structures,[4] leading to remarkable and potentially valuable physicochemical properties.[5,6] In the case of diphenylalanine (FF), the simplest aromatic dipeptide, these crystalline assemblies are often characterized by central voids parallel to and coaxial with the long axes of the crystals,[7,8] even though it has been shown that solid rods can also be fabricated.[9] The crystal structure has been found to be the same irrespective of the overall dimensions of the crystal[10,11] for diameters above 100 nm, and to display a channel containing associated solvent molecules.[5,8]

A wide range of studies have explored possible nanotechnological applications of supramolecular assemblies of FF and its derivatives,[12] resulting in their surface decoration[13,14] and the fabrication of metal nanowires,[14] biosensor electrodes,[15] and optical waveguides.[16] As a structural building block, such micro- and nanoscale peptide structures are very promising, as they are easily prepared, are thermally stable,[17] and possess other unexpected qualities such as piezoelectric behavior[18] and high mechanical strength.[19] Nevertheless, while many of the remarkable properties of the various dipeptide assemblies have been characterized in detail, little is known about the mechanisms by which they self-assemble. Such mechanistic information would be of considerable value as it could lay the foundations for systematic control of the assembly processes.

We have developed an approach for this purpose that is based on a microfluidic flow-reactor, and enables the use of time-resolved optical microscopy to quantify independently the axial and radial growth rates of crystalline assemblies while controlling the chemical potential of the peptide building

Received: May 2, 2016
Published: July 7, 2016

DOI: 10.1021/jacs.6b04136
J. Am. Chem. Soc. 2016, 138, 9589−9596

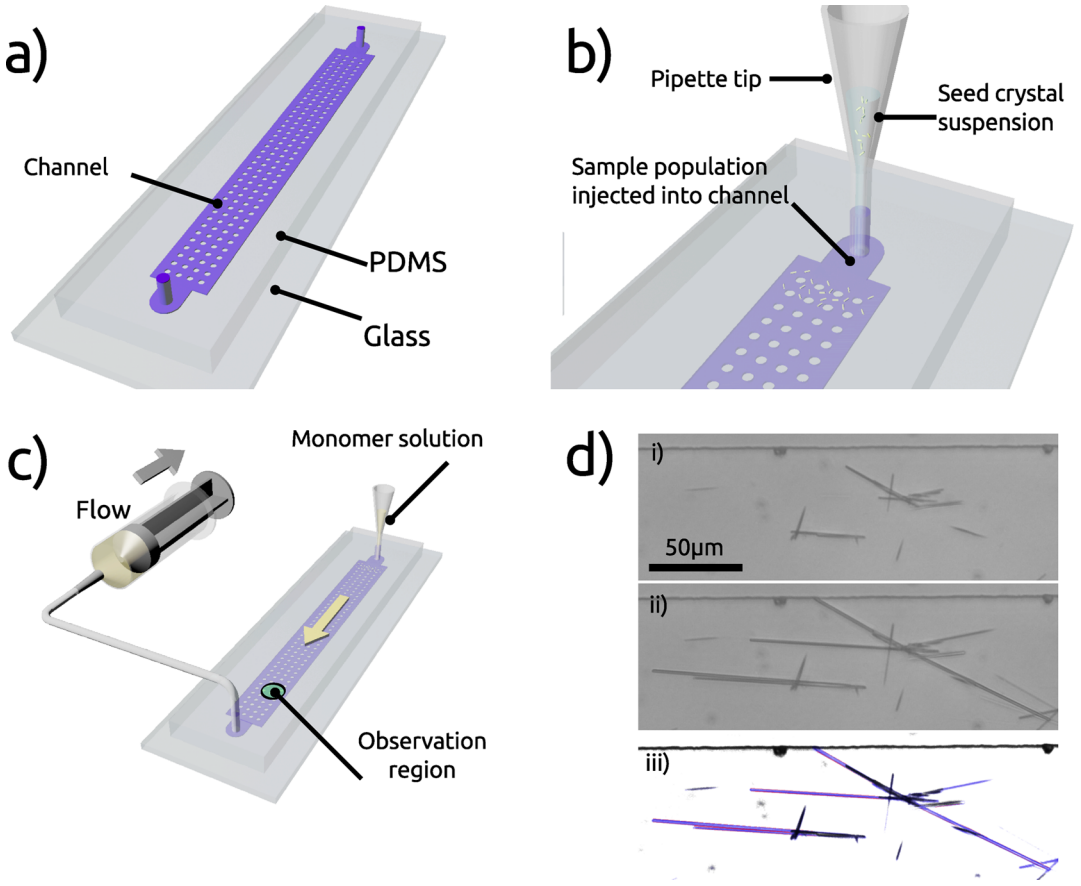

Figure 1. Study of the aggregation kinetics of FF developed in this work using a microfluidic flow reactor. Schematic diagrams illustrate (a) the reactor itself prepared through soft lithography,[22] (b) a suspension of seed crystals being injected into the reactor, (c) supersaturated solution of FF being drawn through the channel by means of a syringe pump at a rate of 800 μL/h, and (d) series of images separated by fixed time periods taken via optical microscopy and changes in the dimensions (blue) recorded. The growth rate is then computed from the five fastest growing crystals in the observation region.

blocks in solution. Furthermore, it is possible to vary rapidly the solution conditions under which growth occurs, as a result of the small volumes of reactants that are used in this approach and the predictability of the flow properties within the reactor.

These results reveal that the growth of FF microcrystals occurs through the nucleation and spread of monolayers on the growing faces of the crystals.[20,21] We show in addition that the varying ratio of axial-to-radial growth rates, resulting from a difference in edge energy between axial and radial nuclei, can be exploited to establish routes to design tubular FF aggregates with controllable aspect ratios, beyond the thermodynamic products.

RESULTS AND DISCUSSION

Kinetics of FF Assembly Measured in a Microfluidic Flow Reactor. We have developed and built a microfluidic flow reactor (Figure 1a), consisting of multiple inlets and a large central chamber with support pillars, which allows the growth kinetics of individual crystalline FF assemblies to be measured via optical time lapse microscopy (Figure 1d). The flow reactor was used to expose the injected, preformed seed crystals (Figure 1b) to a flow of FF solution at a series of constant supersaturation levels (Figure 1c), leading in each case to a distribution of observed growth rates. The growth solutions were maintained at elevated temperature (60−70 °C) to avoid nucleation prior to injection, and the aliquots used for the test runs were extracted and equilibrated rapidly to room temperature, to create a supersaturated solution that was stable, depending on the degree of supersaturation, for up to hours. Measurements of growth kinetics were performed on single ends of individual crystals. The error bars, one standard deviation in width, demonstrate the variation in rates between the five fastest growing crystals (see Experimental Section).

Growth rates were recorded as a function of the solution supersaturation ratio σ, defined as $\sigma = (c - c^*)/c^*$ with c^* the critical concentration. Thus, σ is a dimensionless parameter that expresses the ratio of the concentration c in a given experiment to that under equilibrium conditions, i.e., the critical concentration (for FF at T = 23 °C, its value is c^* = 0.76 g/L = 2.4 mM).[8] The value of σ is zero when $c/c^* = 1$, i.e., when the growth rate of the (semi-infinite) aggregate is zero. The supersaturation ratio σ is related to the free energy of aggregation through the relationship $\Delta G_v = RT\ln(c/c^*) = RT\ln(\sigma + 1)$, where R is the gas constant.

Figure 2a displays the maximum observed growth rates along the long axes of the crystals in units of μm/s. Strikingly, the data in Figure 2a reveal that there is a higher than linear dependence on σ of the axial growth rate (i.e., along the (100) direction, parallel to the long axis of the crystal.

The radial growth rates for FF are shown in Figure 3. As in the case of the axial growth rate, the radial growth rate also depends in a higher than linear manner on σ. Interestingly, the radial growth rate remains at a very low value over a wider

DOI: 10.1021/jacs.6b04136
J. Am. Chem. Soc. 2016, 138, 9589−9596

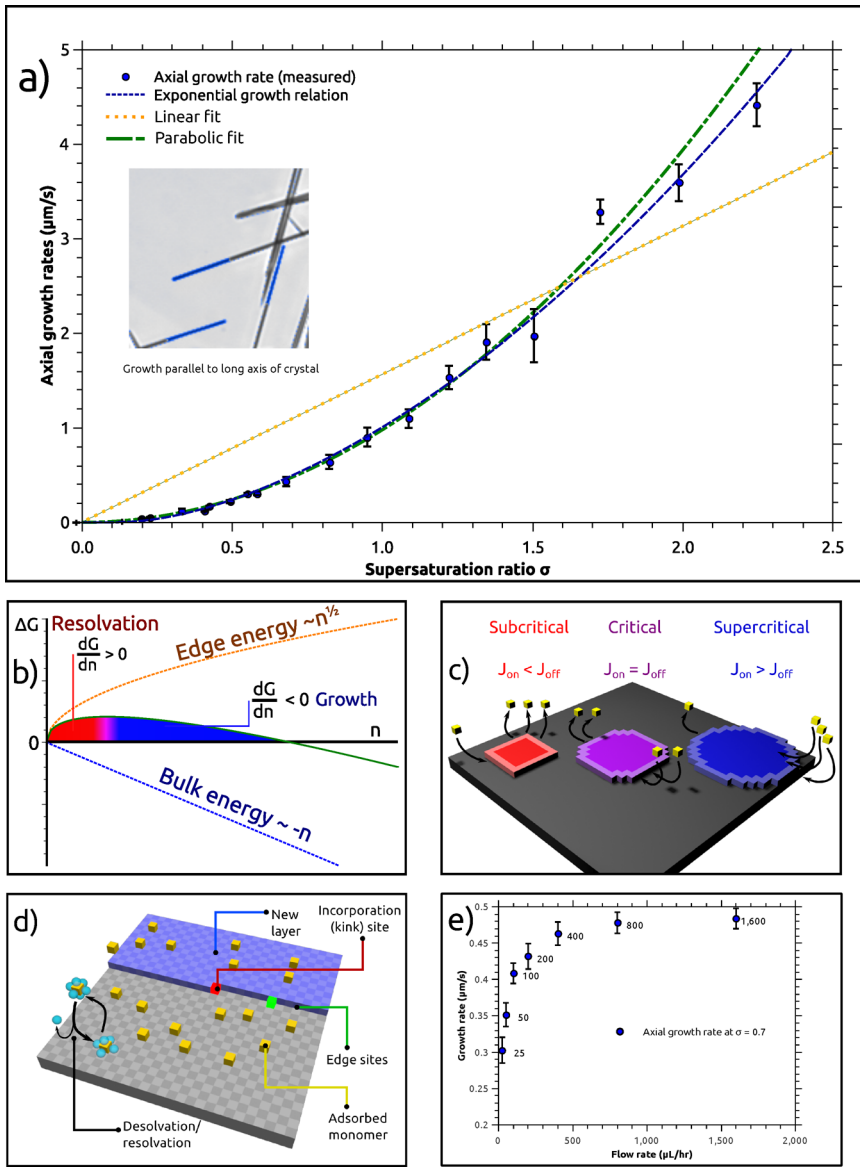

Figure 2. Analysis of axial growth of crystalline FF assemblies. a) Plot of the rate of growth of axial faces of FF crystals as a function of the degree of supersaturation $\sigma = (c - c^*)/c^*$. The blue dashed line is the best-fit curve obtained from the 2D nucleation–growth model.[21] The figure also shows the best fits to the linear (orange dotted line) and parabolic (green dashed dotted line) rate laws. (b) The overall excess free energy of a surface island with n growth units, $G(n)$, has contributions from the edge energy ($\sim n^{1/2}$) and bulk ($\sim n$). Hence, the sum of these two terms has a maximum in correspondence to the critical nucleus size n^* (purple). When $n < n^*$, island growth is unfavorable ($dG/dn > 0$, red), whereas for $n > n^*$ island growth is favorable ($dG/dn < 0$, blue). (c) Schematic representation of nuclei, with edge sites highlighted. Edge sites are coordinatively unsaturated and so have a higher rate of resolvation; the ratio of edge-to-bulk sites determines the nucleus size (n). (d) Representation of features on a simple cubic crystal face. The base crystal is highlighted in gray, the first layer of the crystal is shown in blue and the monomers adsorbed to the surface are shown in yellow. The black arrow denotes a (de)solvation process. Monomers occupying an edge site are highlighted in green, while those occupying a kink site are shown in red. (e) Variation of the growth rate (at $\sigma = 0.7$, 1.3 g/L) as a function of flow rate from 25 to 1600 μL/h in this device. The flow rate of 800 μL/h was chosen, as it was found that the growth rate saturates at this flow rate, and due to greater reliability and lower stresses on the device at the 800 as opposed to 1600 μL/h.

range of values of the supersaturation ratio than does the axial growth rate; indeed, at σ values below $\sigma = 0.4$, radial growth is not detectable, although axial growth is significant. Moreover, the rates of radial growth are ca. 2 orders of magnitude slower than the axial growth rates for all values of σ that were tested.

The Mechanism of Growth of Diphenylalanine Crystalline Assemblies. Crystal growth from solution is a complex process, that involves diffusional arrival of the monomeric building blocks, adsorption onto a growing face, which is usually accompanied by desolvation, followed by surface diffusion until a defect is encountered or by the formation of a two-dimensional nucleus.[21] Each of these processes can be rate determining, depending on the chemical nature and concentrations of the species involved and the solution conditions. For simple inorganic crystals, it has been established that the observed functional dependence of the growth rate on the degree of supersaturation of the solution can be used to decide which of the elementary steps is rate determining.[21]

DOI: 10.1021/jacs.6b04136
J. Am. Chem. Soc. 2016, 138, 9589–9596

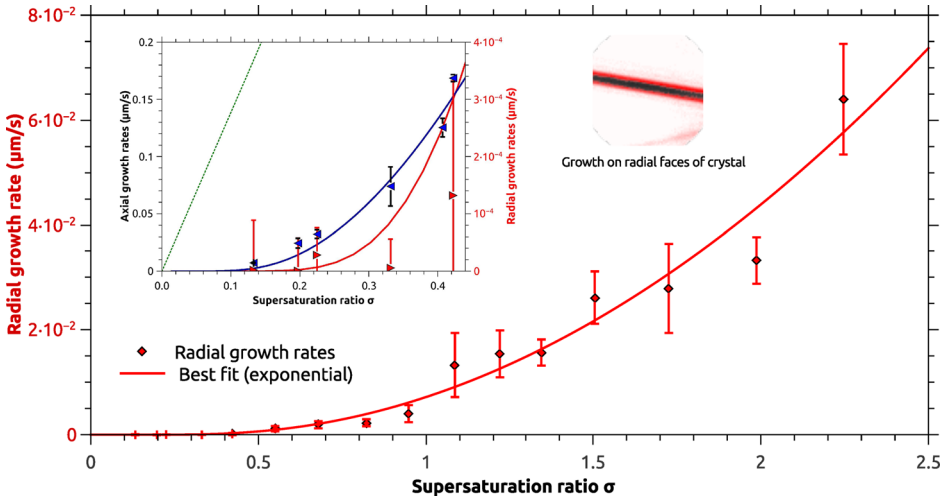

Figure 3. Analysis of radial growth for FF crystals. Radial growth rates of FF crystals as a function of the supersaturation ratio over the range $\sigma = 0$ to $\sigma = 2.25$. Inset: comparison of radial (in red, and right scale) and axial (in blue, and left scale) growth rates. Note that, within experimental error, radial growth is negligible in the σ regime shown in the inset ($\sigma = 0$ to $\sigma = 0.4$).

If the growth rate R_g of a given face is limited by the diffusional arrival of the building blocks, a linear dependence of R_g on σ is anticipated, such that $R_g = k_l\sigma$ with rate constant k_l. The dotted line in Figure 2a shows that a linear relationship of the growth rate on σ, corresponding to a monomolecular or diffusion-limited addition process, does not provide a good fit of the data and hence cannot describe the addition of FF to its crystals. Surface diffusion to defects, such as screw dislocations or kink sites, is expected to yield a parabolic rate law,[21] $R_g = k_p\sigma^2$, with k_p being the rate constant. If, however, the crystal face extends by the 2D-nucleation and subsequent growth (birth-and-spread) of islands, higher-than-quadratic or exponential behavior is predicted.[21] It is difficult, based on the data alone, to distinguish between a parabolic or exponential dependence which yield similarly good fits (Figure 2a, blue and green dashed lines). However, it has been established that growth due to surface defects, such as screw dislocations, is dominant only at very low degrees of supersaturation in most systems.[20] At higher supersaturation ratios, the rate at which addition (kink) sites are formed by the simple presence of high surface concentrations of monomeric subunits is far greater than the rate at which they are formed by addition to pre-existing sites.[20,21] The rate constant k_p entering the parabolic rate low for R_g depends on the individual crystal defect density, which is independent of σ whereas the growth sites are themselves generated in a highly σ-dependent manner in exponential (nucleated) growth. Furthermore, defect-mediated growth is dependent to a large degree on surface diffusion of monomers to kink sites; this process is inhibited in solution growth relative to diffusion from bulk solution.[20,23] Therefore, the defect theory of growth is inconsistent with the wide range over which the growth rate is nonlinear in σ.

By contrast, a nucleation and spread mechanism is able to explain the data in Figures 2 and 3. In this model, the nonlinear relationship between the degree of supersaturation and the growth rate is the result of the balance between the energy cost of creating the coordinatively unsaturated edge sites relative to the energy released by the formation of the more fully coordinated sites in the interior of the nucleus. According to classical nucleation theory,[21] this criticality behavior gives rise to an exponential dependence of the nucleation rate on the surface density of monomers, which is in turn dependent on the relative magnitude of the desolvation/resolvation rates and hence on the degree of supersaturation.[24] To explain the exponential dependence of the rate of growth on σ, we note that the overall excess free energy of a surface island with n growth units is given by[21] $G(n) = 2\gamma(\pi n)^{1/2} - n\Delta G_\nu$, where γ is the edge energy and $\Delta G_\nu = k_B T \log(\sigma + 1)$ is the free energy change of the transformation per growth unit. The first term of $G(n)$ is positive and increases in proportion to $n^{1/2}$, while the second term is negative and varies linearly with n. Hence, as shown in Figure 2b, the sum of these two terms has a maximum value that occurs when $dG/dn = 0$. The value of n at this point is $n^* = \frac{\pi\gamma^2}{\Delta G_\nu^2}$. When $n < n^*$, island growth is unfavorable ($dG/dn > 0$), whereas for $n > n^*$ island growth is favorable ($dG/dn < 0$). Along with this critical nucleus size comes a nucleation barrier of magnitude $G^* = \frac{\pi\gamma^2}{\Delta G_\nu}$ that determines the rate of nucleation $J \sim e^{-G^*/k_B T}$.

If we now define the rate of growth R_g as the inverse time required for nucleated islands to fill up the layer of area A across the growing crystal face, $\tau \sim (JA)^{-1/3}$, we find, using the expression for the nucleation rate above that $R_g \sim (AJ)^{1/3} \sim e^{-K_b/\ln(\sigma+1)}$, where $K_b = \frac{\pi}{3}\left(\frac{\gamma}{k_B T}\right)^2$. The proportionality factor entering this expression for R_g is given explicitly in the Experimental Section and depends on the mechanistic details such as the spacing of lattice sites, the occupation ratio of surface sites in equilibrium and the frequency for diffusional jumps to a stable lattice site.[21] The constant K_b depends on the edge energy γ and can be determined by fitting the experimental kinetic data to the above expression for R_g. From such fits (Figures 2a and 3), we obtain $K_{b,ax} = 0.52 \pm 0.04$, yielding $\gamma_{ax}/k_B T = 0.70 \pm 0.03$ per site for nuclei on the axial face, and $K_{b,rad} = 1.5 \pm 0.3$, yielding $\gamma_{rad}/k_B T = 1.2 \pm 0.12$ per site for nuclei on the radial face. Therefore, a relatively small difference in edge energy of 0.5 $k_B T$ leads to a striking difference of up to 3 orders of magnitude in axial and radial growth rates, and consequently to a highly elongated morphology. The origin of this difference in energy at the

DOI: 10.1021/jacs.6b04136
J. Am. Chem. Soc. 2016, 138, 9589−9596

molecular level can be attributed to the alignment of the charged and polar groups within the crystal structure.[5,8]

It is interesting to contrast the FF microcrystals studied here with amyloid fibrils, micrometer sized filamentous aggregates with diameters in the nanometer range,[25,26] which are formed from polypeptides and proteins. The axial growth rates of FF assemblies measured in this study (addition of monomeric building blocks per time unit) can be compared with those of amyloid fibrils of different proteins (see methods section for details). The result is that the absolute growth rate of FF crystals is close to that of the fastest amyloid fibrils. However, it should be emphasized that the growth of these two types of structures is usually studied at very different absolute concentrations and supersaturations (see Experimental Section).

As mentioned above, amyloid fibrils are not truly one-dimensional structures, but consist of one or more protofilaments.[25,26] It is still unclear whether in a given system individually formed protofilaments associate laterally to form highly ordered, helically twisted mature amyloid fibrils,[27] or whether new protofilaments nucleate on the surface of existing protofilaments.[28] The latter process could be regarded as a special case of the general phenomenon of secondary nucleation, whereby the formation of new assemblies is catalyzed by the surface of existing aggregates.[29] Within a plausible, general picture, if a nucleus forms on the surface of a protofilament or fibril, it can either grow into an additional protofilament, or it can detach and form a new, independent aggregate. In addition, however, individual mature amyloid fibrils can associate laterally,[30,31] especially under solution conditions where the interfilament electrostatic repulsion is screened.[32]

Amyloid fibrils can be regarded as a limiting case of "crystals" with strong axial interactions and weak to negligible radial interactions $\gamma_{rad} - \gamma_{ax} \gg 0.5\ k_BT$, leading to filamentous morphology, and the ability to proliferate through secondary nucleation.[29] In small molecule crystals, the equilibrium morphology of the solid phase is predictable from the Gibbs–Wulff theorem,[33] which states that the higher energy faces of a crystal grow faster, and so the faces normal to these high-energy interactions will be further from the centroid of the crystal at equilibrium. Therefore, the equilibrium aspect ratio of a crystal is determined by the relative energies of the faces and cannot easily be modified, unless a drastic change in solution conditions, in particular solvent composition, is employed.[8]

Morphological Control of Dipeptide Supramolecular Polymers. Variations in crystal morphology and aspect ratio have been achieved for inorganic crystals[34,35] through control of the degree of solution supersaturation. The extended metastability of supercooled FF solutions at high concentrations allows the degree of solution supersaturation to be varied over a wide range, suggesting that the morphology of FF assemblies might be varied through the control of supersaturation. As FF is the subject of much research into possible applications in materials science,[14,36−38] the ability to tune aspect ratios of these crystalline supramolecular assemblies is of great importance.[15,39] Based on our conclusions concerning the growth mechanism and its dependence on supersaturation, experiments were designed with the goal of growing the assemblies in a regime in which only axial growth can occur at a significant rate, and to compare the aspect ratios of the resulting assemblies with those that are grown under conditions permitting both axial and radial growth. The use of a flow reactor makes it possible to maintain the system under a nonequilibrium condition, in which the crystal dimensions are not determined by the equilibrium solubilities of each face, but rather by the respective growth rates,[40,41] opening up the possibility of kinetic rather than purely thermodynamic control of peptide self-assembly.

To establish the applicability of the findings described above to the controlled growth of populations of FF microcrystalline assemblies, an experiment was devised to prepare initial samples of highly homogeneous crystals and then to grow them in a device with removable plug, allowing opening and resealing to enable the recovery of samples after exposure to the supersaturated solutions (Figure 4a). Comparison of the distributions of length and width before and after exposure to a given growth condition demonstrates the controlled increase in aspect ratio possible at a low level of supersaturation ratio (σ = 0.31), where the solution conditions are maintained by continuous flow; under these conditions, no radial growth was detectable within experimental error. The rapid growth at a higher supersaturation ratio (σ = 1.46) results in radial growth occurring simultaneously with axial growth. From an initial suspension of microcrystals with a given distribution of radial dimensions, this distribution can be maintained while the crystals undergo solely axial growth (Figure 4b and e), or it can be increased (Figure 4c and d) simultaneously with axial growth. The crystals so modified are easily recovered from the device through resuspension in a saturated solution, or in a liquid in which the dipeptide is practically insoluble, e.g., hexane or perfluorocarbons.[8]

■ CONCLUSIONS

We have found that detailed mechanistic analysis, made possible by the application of microfluidic techniques described here, reveals that crystalline FF supramolecular polymers grow in aqueous solution by a process of 2D surface nucleation (2DN), and that the formation of these nuclei, and hence the generation of growth sites on the surface, is rate determining at all the levels of solution supersaturation that were explored in this study. There are differences between axial and radial growth rates in FF as a result of the very different surface free energies characteristic of each face. The relative growth rates of the axial and radial faces of the FF microcrystals have been found to be adjustable through simple control of the supersaturation levels of the solutions in microfluidic flow reactors. This conclusion has enabled us to develop procedures for the controlled modification of the aspect ratio beyond the value dictated by thermodynamics, and for the transfer of populations of crystalline assemblies for further processing. The overall morphology of such dipeptide supramolecular polymers is of great significance in the context of their applications as scaffolds or actuators for a variety of complex nanoscale structures, and the ability to control the aspect ratio of the structures enables in a simple manner to tune the physical properties of the assemblies.

■ EXPERIMENTAL SECTION

Microfluidics. The flow reactors used in this study were microfluidic devices constructed from polydimethylsiloxane (PDMS), according to standard protocols of soft lithography.[22,42] In brief, a 25 μm thick layer of SU-8 3025 photoresist was spin-coated onto a silicon wafer, exposed to UV-light through a mask in which the device design was printed, then manufactured in 1-methoxy-2-propyl acetate (PGMEA). The microfluidic device was fabricated from Sylgard 184

DOI: 10.1021/jacs.6b04136
J. Am. Chem. Soc. 2016, 138, 9589−9596

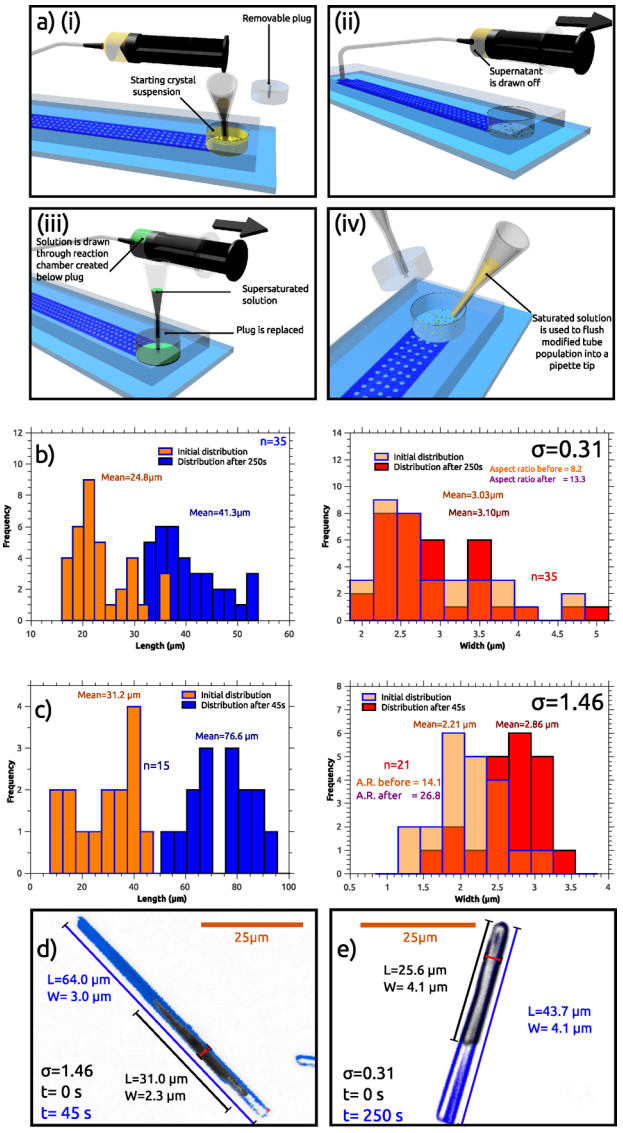

Figure 4. Morphology control in a nonequilibrium flow reactor setup a) Schematic representation of a bulk microfluidic reactor. (i) A homogenized suspension of FF crystals is introduced into the channel through a broad well that is generated by the removal of a circular plug. (ii) The supernatant is drawn off with a syringe pump. (iii) The plug is reinserted generating a second reservoir containing a solution of known supersaturation (green). This solution is drawn over the bed of the reactor by the syringe pump. (iv) The modified crystals are flushed into a pipet tip for further processing and study. (b,c) The results of this experiment indicate the development of the populations of crystals measured *in situ* without removal from the device. (b) Length and width distributions before and after exposure for 250 s to a flow of FF solution at $\sigma = 0.31$. Average aspect ratio changes from 8.2 to 13.3 during the 250 s run. (c) Length and width distributions before and after exposure for 45s to a solution at $\sigma = 1.46$. Aspect ratio changes on average from 14.1 to 26.8 in 45 s. Some crystals grew outside of the observed area during this run, therefore the length histograms do not feature the same number of data points before and after the incubation with monomer. (d) Illustration of a crystal that has undergone both axial and radial growth at $\sigma = 1.46$. (e) At $\sigma = 0.31$, only axial growth is observed.

PDMS elastomer (DowCorning, Midland, MI), using 1 h curing at 65 °C. After cutting the device, punching the holes for inlets and outlets, and activation via plasma treatment with a Femto plasma bonder (Diener Electronic, Ebhausen, Germany), the microfluidic device was bonded to a 3 × 1 in. microscope slide. A suspension of seed crystals was passed through the device, and once sufficient crystals had settled in the central chamber, a flow of solution of known concentration was initiated at a rate of 800 μL/h, corresponding to velocities on the order of millimeters per second in the channel center, by means of a neMESYS syringe pump (Cetoni, Korbussen, Germany). The experiment was halted either at the predetermined time or if nucleation was observed in the supersaturated solution.

Measurements of lengths of growing microcrystals were made every 5 s using time delay photography, using a Zeiss Axio Observer A1 microscope (Carl Zeiss, Jena, Germany) and a CoolSNAP-MYO camera (Photometrics, Tucson, AZ). For the experimental long time scales used in the morphology-control experiments, images were taken every 5 min for periods up to 1000 min. To ensure sufficient sample population of growing crystals, suspensions of seed crystals were injected into the channel and the supernatant drawn off leaving large numbers of settled crystals. The results were recorded after a delay of 60 min after commencing flow, in order to limit the influence of the resolvation of small aggregates.

The axial and radial growth rates at each value of the supersaturation were computed as the mean ± standard deviation of the five fastest growing structures. We included only the five fastest growing crystals in order to ensure that the reaction was not inhibited by random effects arising from positioning, surface contact or contamination, which would be expected to slow down the growth kinetics. This strategy was prompted by the observation that even at the highest values of σ, some crystals displayed no measurable growth. The kinetic data (growth rate as a function of σ) were fitted to the exponential model derived by Nielsen[21] for 2D-nucleation dominated crystal growth. This analysis has the caveat that there is possibly an additional contribution from a dislocation mechanism, that will be more important at low σ values, but is generally likely to be very small.[21]

Solutions and Seed Crystals. Solutions in water were prepared by the suspension of FF (diphenylalanine, Bachem, Bubendorf, Switzerland) in distilled water (18.2 MΩ/m) followed by ultrasonication in a sonic bath until the suspension was homogeneous, and then heating to 100 °C. Following incubation for 30 min at this temperature, no visible aggregates were observable for concentrations up to and including 6 g/L (19.2 mM); these solutions were then diluted to the desired concentrations for the growth experiments. To confirm the concentrations, the absorbance at 258 nm at room temperature was taken to be proportional to concentration (absorption coefficient of FF at 258 nm is 390 cm^{-1} M^{-1}). These measurements were made using a Cary 400 spectrophotometer, instrument version 8.01. Spectra were recorded between 300 and 230 nm with a reading every 0.4 nm with a spectral bandwidth of 2 nm, using glass cuvettes with 10 mm path lengths. Concentrations were taken to be proportional to the peak height of the absorption maximum closest to 258 nm.

Preformed seed fibrils were prepared for growth experiments by cooling-induced precipitation of 2 g/L FF from dd H_2O. The resultant suspensions were kept cool and sonicated (Sonorex, 50% power, 50% duty cycle, 2 min, Bandelin, Berlin, Germany) prior injection into the channels by micropipette through the outlet port of the microfluidic device. Suspensions of microcrystals, with a relatively narrow starting size distribution, for the experiments in which the aspect ratios were modified were prepared by sonication of 1 mL of an aggregated suspension at 2g/L total FF concentration without external cooling (Bandelin Sonorex, 50% power, 50% duty cycle, 2 min).

Relationship between Growth Rate and Supersaturation Ratio. The exact exponential relationship between the growth rate and σ that is predicted by classical nucleation theory[21] can be expressed as $R_g = k_e(\sigma + 1)^{7/6}\sigma^{2/3}(\ln(\sigma + 1))^{1/6}\, e^{-K_b/\ln(\sigma+1)}$, where $k_e = 2a\nu_{in}(K_{ad}c^*V_m)^{4/3}\, e^{-\gamma/k_BT}$ and $K_b = \frac{\pi}{3}\left(\frac{\gamma}{k_BT}\right)^2$. In this expression, a is the lattice site spacing, ν_{in} is the integration jump frequency (incorporating the desolvation step) for the diffusional jump to a stable (kink) lattice site, γ is the edge energy, and K_{ad} is the

DOI: 10.1021/jacs.6b04136
J. Am. Chem. Soc. 2016, 138, 9589−9596

equilibrium constant for adsorption to the surface. The term $K_{ad}c^*V_m$ therefore represents the occupation ratio of surface sites in equilibrium with the solution.[21] The values for the rate constant k_e and the parameter K_b obtained from the fit of the axial and radial experimental kinetic data were determined tobe $k_{e,ax} = 1.02 \pm 0.06$ μm/s and $K_{b,ax} = 0.52 \pm 0.04$, yielding $\gamma_{ax}/k_BT = 0.70 \pm 0.03$ per site for nuclei on the axial face, and $k_{e,rad} = 0.03 \pm 0.01$ μm/s and $K_{b,rad} = 1.5 \pm 0.3$, yielding $\gamma_{rad}/k_BT = 1.2 \pm 0.12$ per site for nuclei on the radial face.

An alternative approach to the theory of island growth[21] expresses the growth rate R_g as a power law with respect to supersaturation, $R_g = k_n\sigma^{n_c}$.[43] In this expression, k_n represents the rate constant for nucleation while n_c is the reaction order for the nucleation process, which relates to the size n^* of the critical nucleus as $n_c = n^* - 1$. Both the classical nucleation theory and the empirical approaches are based upon a clustering mechanism of reacting particles,[44] but they assume a different effect of the degree of supersaturation on the size of the critical nucleus. Classical nucleation theory indicates that the critical size n^* is dependent on the degree of supersaturation, $n^* = \pi\gamma^2/(k_BT\log(\sigma + 1))^2$, whereas the empirical theory discussed above assumes a constant nucleus size, $n^* = n_c + 1$. Fitting the experimentally measured growth rates to the empirical power law not only shows good overall agreement of the data with the empirical nucleation model, but the reaction orders determined from the analysis, $n_{c,ax} \sim 1.8$ for axial growth and $n_{c,rad} \sim 3.3$ for radial growth, are also consistent with the values for the line energy γ determined using classical nucleation theory. Thus, using the latter theory for the supersaturation values of $\sigma \sim 1.1$ and $\sigma \sim 1.8$, respectively, predicts $n^*_{ax} \sim 2.8$ and $n^*_{rad} \sim 4.3$. This alternative empirical approach suggests, therefore, that small differences in edge energies between axial and radial growth can be interpreted in terms of different sizes of nuclei for both growth directions, thus providing a geometrical interpretation for the elongated morphology.

Computation of Molecular Growth Rate of FF Crystals and Comparison with Those of Amyloid Fibrils. From Figure 2a, we can see that that axial growth rate is 1 μm/s at a supersaturation $\sigma = 1$, which corresponds to a monomer concentration of 1.52 g/L,[8] or 4.866 mM. For simplicity, we take the unit cell dimension in the axial direction, 4.9 Å, as the size of one molecule inside the crystal.[8] The growth rate of 1 μm/s then corresponds to 2041 FF molecules adding per second in axial dimension. Of course this has to be multiplied, for any given crystal, with the number of molecules in the cross-section of this crystal. For the sake of comparison with an amyloid fibril, however, we limit our discussion to the purely one-dimensional growth rate. This value of the growth rate can be compared with that of typical amyloid fibrils, such as those formed from the amyloid β 42 peptide. For this peptide, the elongation rate constant has been reported to be 3×10^6 s^{-1} M^{-1}. Under the (simplifying[45]) assumption that the amyloid fibril elongation rate is linear in monomer concentration up to 4.866 mM, the molecular elongation rate at this concentration would be 14 598 molecules of Aβ 42 molecules per second, a value seven times higher than for the FF dipeptide. Experiments with the amyloid β peptide are usually performed at 1000 times lower concentration (ca. 5 μM), which corresponds to a supersaturation of $\sigma = 25$.[46] As a second example, we use the protein α-synuclein, the elongation rate constant of which has been reported to be of the order of 2×10^3 s^{-1} M^{-1}.[32] This yields an elongation rate of 10 molecules of α-synuclein per second at 4.866 mM, again under the assumption, for the sake of easy comparability, that the elongation rate is linear in the monomer concentration up to the mM range. However, it has been shown that this linearity no longer holds above 100 μM.[32] Similarly to the amyloid β peptide, alpha-synuclein is usually studied at supersaturation values of 25−50 (critical concentration is of the order of 1 μM[47]).

Therefore, it can be concluded that the axial rate of FF assembly is comparable to the rate of elongation of the fastest growing amyloid fibrils, such as those of the Aβ peptide.

AUTHOR INFORMATION

Corresponding Authors

*alexander.buell@uni-duesseldorf.de

*tpjk2@cam.ac.uk

Notes

The authors declare no competing financial interest.

ACKNOWLEDGMENTS

We thank the Newman Foundation (T.O.M. and T.P.J.K.), St. John's College Cambridge (T.C.T.M.), the ERC (T.C.T.M. and T.P.J.K.), the BBSRC (T.P.J.K.), FEBS and EMBO (A.L.), the Tel Aviv University Center for Nanoscience and Nanotechnology (A.L.), the Israeli National Nanotechnology Initiative and Helmsley Charitable Trust (E.G.), Elan Pharmaceuticals (C.M.D., T.P.J.K., T.O.M., and A.K.B.) and the Daniel Turnberg foundation (A.K.B.), Leverhulme Trust (A.K.B.), and Magdalene College (A.K.B.) for financial support. T.O.M. would further like to thank Dr. Mark Eddleston for valuable discussions.

REFERENCES

(1) Aida, T.; Meijer, E. W.; Stupp, S. I. *Science* **2012**, *335*, 813−817.

(2) Tysseling-Mattiace, V. M.; Sahni, V.; Niece, K. L.; Birch, D.; Czeisler, C.; Fehlings, M. G.; Stupp, S. I.; Kessler, J. A. *J. Neurosci.* **2008**, *28*, 3814−3823.

(3) Marshall, K. E.; Hicks, M. R.; Williams, T. L.; Hoffmann, S. V.; Rodger, A.; Dafforn, T. R.; Serpell, L. C. *Biophys. J.* **2010**, *98*, 330−338.

(4) Levin, A.; Mason, T. O.; Adler-Abramovich, L.; Buell, A. K.; Meisl, G.; Galvagnion, C.; Bram, Y.; Stratford, S. A.; Dobson, C. M.; Knowles, T. P. J.; Gazit, E. *Nat. Commun.* **2014**, *5*, 5219.

(5) Görbitz, C. H. *Chem. - Eur. J.* **2001**, *7*, 5153−5159.

(6) Reches, M.; Gazit, E. *Science* **2003**, *300*, 625−627.

(7) Görbitz, C. H. *Chem. Commun. (Cambridge, U. K.)* **2006**, 2332−2334.

(8) Mason, T. O.; Chirgadze, D. Y.; Levin, A.; Adler-Abramovich, L.; Gazit, E.; Knowles, T. P. J.; Buell, A. K. *ACS Nano* **2014**, *8*, 1243−1253.

(9) Li, Q.; Jia, Y.; Dai, L.; Yang, Y.; Li, J. *ACS Nano* **2015**, *9*, 2689−2695.

(10) Lekprasert, B.; Sedman, V.; Roberts, C. J.; Tedler, S. J. B.; Notingher, I. *Opt. Lett.* **2010**, *35*, 4193−4195.

(11) Lekprasert, B.; Korolkov, V.; Falamas, A.; Chis, V.; Roberts, C. J.; Tendler, S. J. B.; Notingher, I. *Biomacromolecules* **2012**, *13*, 2181−2187.

(12) Yan, X.; Zhu, P.; Li, J. *Chem. Soc. Rev.* **2010**, *39*, 1877−1890.

(13) Reches, M.; Gazit, E. *J. Nanosci. Nanotechnol.* **2007**, *7*, 2239−2245.

(14) Carny, O.; Shalev, D. E.; Gazit, E. *Nano Lett.* **2006**, *6*, 1594−1597.

(15) Yemini, M.; Reches, M.; Gazit, E.; Rishpon, J. *Anal. Chem.* **2005**, *77*, 5155−5159.

(16) Yan, X.; Su, Y.; Li, J.; Früh, J.; Möhwald, H. *Angew. Chem., Int. Ed.* **2011**, *50*, 11186−11191.

(17) Adler-Abramovich, L.; Reches, M.; Sedman, V.; Allen, S.; Tendler, S. J. B.; Gazit, E. *Langmuir* **2006**, *22*, 1313−1320.

(18) Gour, N.; Barman, A. K.; Verma, S. *J. Pept. Sci.* **2012**, *18*, 405−412.

(19) Niu, L.; Chen, X.; Allen, S.; Tendler, S. J. B. *Langmuir* **2007**, *23*, 7443−7446.

(20) Burton, W. K.; Cabrera, N.; Frank, F. C. *Philos. Trans. R. Soc., A* **1951**, *243*, 299−358.

(21) Nielsen, A. E. *J. Cryst. Growth* **1984**, *67*, 289−310.

(22) Duffy, D. C.; McDonald, J. C.; Schueller, O. J.; Whitesides, G. M. *Anal. Chem.* **1998**, *70*, 4974−4984.

DOI: 10.1021/jacs.6b04136
J. Am. Chem. Soc. 2016, 138, 9589−9596

(23) Chernov, A. A. *Prog. Cryst. Growth Charact. Mater.* **1993**, *26*, 121−151.
(24) Lewis, B. *J. Cryst. Growth* **1974**, *21*, 40−50.
(25) Ban, T.; Hoshino, M.; Takahashi, S.; Hamada, D.; Hasegawa, K.; Naiki, H.; Goto, Y. *J. Mol. Biol.* **2004**, *344*, 757−767.
(26) Fitzpatrick, A. W. P.; Debelouchina, G. T.; Bayro, M. J.; Clare, D. K.; Caporini, M. A.; Bajaj, V. S.; Jaroniec, C. P.; Wang, L.; Ladizhansky, V.; Müller, S. A.; MacPhee, C. E.; Waudby, C. A.; Mott, H. R.; De Simone, A.; Knowles, T. P. J.; Saibil, H. R.; Vendruscolo, M.; Orlova, E. V.; Griffin, R. G.; Dobson, C. M. *Proc. Natl. Acad. Sci. U. S. A.* **2013**, *110*, 5468−5473.
(27) Bolisetty, S.; Adamcik, J.; Mezzenga, R. *Soft Matter* **2011**, *7*, 493−499.
(28) Jeong, J. S.; Ansaloni, A.; Mezzenga, R.; Lashuel, H. A.; Dietler, G. *J. Mol. Biol.* **2013**, *425*, 1765−1781.
(29) Cohen, S. I. A.; Linse, S.; Luheshi, L. M.; Hellstrand, E.; White, D. A.; Rajah, L.; Otzen, D. E.; Vendruscolo, M.; Dobson, C. M.; Knowles, T. P. J. *Proc. Natl. Acad. Sci. U. S. A.* **2013**, *110*, 9758−9763.
(30) Petkova, A. T.; Leapman, R. D.; Guo, Z.; Yau, W.-M.; Mattson, M. P.; Tycko, R. *Science* **2005**, *307*, 262−265.
(31) Jansen, R.; Dzwolak, W.; Winter, R. *Biophys. J.* **2005**, *88*, 1344−1353.
(32) Buell, A. K.; Galvagnion, C.; Gaspar, R.; Sparr, E.; Vendruscolo, M.; Knowles, T. P. J.; Linse, S.; Dobson, C. M. *Proc. Natl. Acad. Sci. U. S. A.* **2014**, *111*, 7671−7676.
(33) Wulff, G. *Z. Kristallogr. - Cryst. Mater.* **1901**, *34*, 449−530.
(34) Takubo, H.; Kume, S.; Koizumi, M. *J. Cryst. Growth* **1984**, *67*, 217−226.
(35) Li, S.; Xu, J.; Luo, G. *J. Cryst. Growth* **2007**, *304*, 219−224.
(36) Yan, X.; Cui, Y.; He, Q.; Wang, K.; Li, J. *Chem. Mater.* **2008**, *20*, 1522−1526.
(37) Souza, M. I.; Jaques, Y. M.; de Andrade, G. P.; Ribeiro, A. O.; da Silva, E. R.; Fileti, E. E.; Ávilla, E. D. S.; Pinheiro, M. V. B.; Krambrock, K.; Alves, W. a. *J. Phys. Chem. B* **2013**, *117*, 2605−2614.
(38) Levin, A.; Michaels, T.; Adler-Abramovich, L.; Mason, T. O.; Müller, T.; Zhang, B.; Mahadevan, L.; Gazit, E.; Knowles, T. P. J. *Nat. Phys.* **2016**, DOI: 10.1038/nphys3808.
(39) Andersen, K. B.; Christiansen, N. O.; Castillo-León, J.; Rozlosnik, N.; Svendsen, W. E. *Org. Electron.* **2013**, *14*, 1370−1375.
(40) Chernov, A. *Sov. Phys. Crystallogr.* **1963**, *7*, 728−730.
(41) Gadewar, S. B.; Doherty, M. F. *J. Cryst. Growth* **2004**, *267*, 239−250.
(42) Whitesides, G. M. *Nature* **2006**, *442*, 368−373.
(43) Nielsen, A. E. *Kinetics of Precipitation*; Pergamon Press: Oxford, New York, 1964.
(44) Zeldovich, Y. Zh. *Eksp. Teor. Fiz. (Russian)* **1942**, *12*, 525.
(45) Buell, A. K.; Blundell, J. R.; Dobson, C. M.; Welland, M. E.; Terentjev, E. M.; Knowles, T. P. J. *Phys. Rev. Lett.* **2010**, *104*, 228101.
(46) Hellstrand, E.; Boland, B.; Walsh, D. M.; Linse, S. *ACS Chem. Neurosci.* **2010**, *1*, 13−18.
(47) Baldwin, A. J.; Knowles, T. P. J.; Tartaglia, G. G.; Fitzpatrick, A. W.; Devlin, G. L.; Shammas, S. L.; Waudby, C. A.; Mossuto, M. F.; Meehan, S.; Gras, S. L.; Christodoulou, J.; Anthony-Cahill, S. J.; Barker, P. D.; Vendruscolo, M.; Dobson, C. M. *J. Am. Chem. Soc.* **2011**, *133*, 14160−14163.

DOI: 10.1021/jacs.6b04136
J. Am. Chem. Soc. 2016, 138, 9589−9596